

Methodology study of machine learning for the neutron star equation of state

Yuki Fujimoto, Kenji Fukushima, and Koichi Murase
*Department of Physics, The University of Tokyo,
7-3-1 Hongo, Bunkyo-ku, Tokyo 113-0033, Japan*

We discuss a methodology of machine learning to deduce the neutron star equation of state from a set of mass-radius observational data. We propose an efficient procedure to deal with a mapping from finite data points with observational errors onto an equation of state. We generate training data and optimize the neural network. Using independent validation data (mock observational data) we confirm that the equation of state is correctly reconstructed with precision surpassing observational errors. We finally discuss the relation between our method and Bayesian analysis with an emphasis put on generality of our method for underdetermined problems.

The equation of state (EoS) of dense nuclear and quark matter should be derived from quantum chromodynamics (QCD), but the sign problem in dense QCD prevents us from the first principles calculation [1]. It is unlikely that the conventional nuclear EoS in terms of nucleons keeps validity in deep cores of the neutron star (see Ref. [2] for a review). If we use a typical nuclear EoS to realize a two solar mass neutron star [3], the central density could exceed several times ρ_0 , where ρ_0 represents the nuclear mass density at the saturation point, i.e. $\rho_0 \simeq (\text{nucleon mass}) \times 0.16 [\text{nucleon}/\text{fm}^3] \simeq 2.7 \times 10^{14} [\text{g}/\text{cm}^3]$. Novel phases of matter are expected at such high density, but there is no established description for a transition between various matter. High temperature QCD phases (see Ref. [4] for recent reviews) have inspired a continuous crossover scenario from nuclear to quark degrees of freedom [5], which is called quark-hadron continuity [6].

Our knowledge is limited and we need scenario independent approaches to neutron star studies. To this end experimental information would be useful to constrain possible EoS candidates. We have such valuable experimental data of the neutron star mass M and radius R , and the M - R points from neutron star observations would ideally shape a curve called the M - R relation [7].

The one-to-one correspondence between the M - R relation and the EoS is, *formally*, mediated by the Tolman-Oppenheimer-Volkoff (TOV) equation [8] coupled with $dm/dr = 4\pi\rho r^2$ where r is the radial distance, ρ is the mass density, and m is the mass within the radius- r sphere. Specifically, the EoS refers to $\rho = \rho(p)$ with p being the pressure (where neglecting rotation and magnetic effects are assumed; see Ref. [9] for a modified EoS). The TOV equation is a differential equation for $p(r)$ and $\rho(r)$. The radius R is fixed by $p(r = R) = 0$, and the mass is given by $M = m(R)$. It is possible to solve the TOV equation from the M - R relation to the EoS (up to some critical density) as discussed in Ref. [10].

However, *practically*, we do not know the M - R relation with arbitrary precision from neutron star observations. To complicate matters, a third family scenario may be realized [11, 12]. Thus, instead of revealing the unique EoS from the M - R curve, we construct the most likely

EoS from discrete M - R points. We should develop a robust approach to deal with observational M - R points that deviate from the genuine M - R relation with errors.

One strategy is as follows. First, we setup an EoS with several parameters (such as parametrized spectral function of relativistic enthalpy [13], piecewise polytropic parametrization [14], etc). Then, we proceed to determine parameters by making the outputs closest to the observational data. This approach works for the current problem with only discrete observational points, but it is nontrivial how to estimate the parametrization dependence systematically.

It would be desirable to establish some alternative method in a systematic way. Along these lines, recently, a method based on the Bayesian analysis has attracted theoretical interest [15–17]. In Bayesian analysis a certain prior distribution of EoS is prepared, and Bayesian updating for the EoS distribution is made by the M - R observations. The EoS parametrization dependence is incorporated in the prior dependence, and can be quantified by comparing different priors. In principle, if the number of the M - R data points is sufficiently large, the prior distribution dependence can be arbitrarily suppressed.

The purpose of this work is to address another method, which is complementary to Bayesian analysis and is straightforwardly implemented numerically. We will introduce a new principle to infer the neutron star EoS utilizing deep (i.e. many-layered) neural network of machine learning, which has been successfully applied to QCD and nuclear physics [18, 19]. Throughout this paper, we use the natural unit; $c = G = 1$.

Here, we make a brief overview on machine learning and deep neural network. This method provides a handy and powerful way to find an optimized mapping expressed in the “neural network” model. For the “supervised” learning, we first prepare “training data”, that is, data sets of input and output, and then optimize the parameter set of the mapping from input to output. Once the optimization is sufficiently achieved or the training is complete, the neural network model can conversely make an educated guess about the most likely output corre-

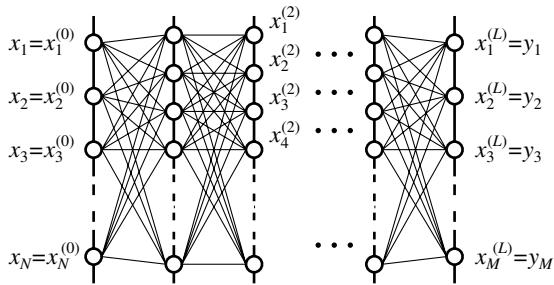


FIG. 1. Feedforward neural network.

sponding to a given input. The advantage of machine learning, as compared to ordinary fitting procedures, is that we need not rely on preknowledge about fitting functions because the multi layer structures are capable of capturing any functions.

The model function of feedforward neural network can be expressed as follows:

$$y_i = f_i(\{x_j\} | \{W_{jk}^{(1)}, a_j^{(1)}, \dots, W_{jk}^{(L)}, a_j^{(L)}\}), \quad (1)$$

where $\{x_i\}$ and $\{y_i\}$ are input and output data, respectively. We setup $L + 1$ layers (including the input and the output layers). Fitting parameters, $\{W_{ij}^{(k)}, a_i^{(k)}\}$, on the k -th layer, denote the weights between nodes in two adjacent layers and the activation offset at each node [see Eq. (2)]. For the zeroth layer, the input is set as $x_i^{(0)} = x_i$ ($1 \leq i \leq N_1$) with N_1 being the size of input $\{x_i\}$. For the subsequent layers, the transformations are iteratively applied as

$$x_i^{(k+1)} = \sigma^{(k+1)} \left(\sum_{j=1}^{N_k} W_{ij}^{(k+1)} x_j^{(k)} + a_i^{(k+1)} \right), \quad (2)$$

which defines f_i , where $1 \leq i \leq N_{k+1}$ with N_{k+1} being the node numbers. The final output from the L -th layer is $y_i = x_i^{(L)}$ ($1 \leq i \leq N_L$) with N_L being the size of output $\{y_i\}$. Here, $\sigma^{(k)}(x)$'s are called ‘‘activation functions’’ and the typical choices include the sigmoid function $\sigma(x) = 1/(e^x + 1)$, the ReLU $\sigma(x) = \max\{0, x\}$, hyperbolic tangent $\sigma(x) = \tanh(x)$, etc. The general design structure is schematically depicted in Fig. 1, in which the calculation proceeds from the left with input $\{x_i\}$ to the right with output $\{y_i\}$.

For the actual optimization procedure we choose a ‘‘loss function’’ to be minimized; if the loss function is the mean square deviation, the learning amounts to the standard least square method with f_i expressed by neural network.

For better learning, the training data quality is important. For the training purpose we should not bias data from physical reasonability, and intuitively unnatural data should be also included to raise more adaptive

neural network. Now, let us explain how we have prepared training data which consist of randomly generated EoS and corresponding observational points, (M_i, R_i) .

First, we elucidate our scheme for the EoS generation (see Ref. [20] for details). Up to the density ρ_0 , we use a conventional nuclear EoS (i.e. SLy [21] in this study), and a range $[\rho_0, 8\rho_0]$ is equally partitioned in logarithmic scale into five segments. We randomly assign the average sound velocity $dp/d\rho = c_s^2$ to five segments according to the uniform distribution within $0.02 < c_s^2 < 0.98$ where a small margin by 0.02 is a regulator to avoid singular behavior of the TOV equation. From these sound velocities we determine the pressure values at segment boundaries. We interpolate the EoS inside of each segment assuming polytrope $p \propto \rho^\Gamma$. We note that we allow for small c_s^2 corresponding to a (nearly) first-order phase transition. We generated 2000 EoSs in this way.

Next, we solve the TOV equation [8] using the generated $p(\rho)$ from $m = r = 0$ and the enthalpy density $h = h_c$ (where h_c is a free parameter corresponding to a choice of the central core density) until h hits zero (see Ref. [10] for the formulation using h). Then, we identify $M = m(h = 0)$ and $R = r(h = 0)$, so that (M, R) with various h_c gives the M - R curve. For each randomly generated EoS we get the M - R curve and identify the maximum mass M_{\max} . If M_{\max} does not reach the observed mass [i.e. $1.97M_\odot$ from the lower bound of $(2.01 \pm 0.04)M_\odot$ [3] where M_\odot denotes the solar mass], such EoSs are rejected from the ensemble. In this work 52 out of 2000 EoSs are rejected (1948 remaining).

Then, for each EoS and corresponding M - R relation, we sample 15 observational (M_i, R_i) . Here, this choice of 15 is simply for the demonstration purpose, so it should be adjusted according to the number of available neutron star observations (which is so far 18 and increasing in the future [7]). For better training quality, we should make unbiased sampling of 15 data points, and we assume a uniform distribution of M over $[M_\odot, M_{\max}]$. If there are multiple values of R corresponding to one M , we always take larger R discarding unstable branches. In this way, we select 15 points of $(M_i^{(0)}, R_i^{(0)})$ on the M - R relation. We also train neural network to learn that real observational data contain errors, ΔM and ΔR , which makes data points departed away from the genuine M - R relation. We randomly generate ΔM_i and ΔR_i according to the normal distribution with variances, $0.1M_\odot$ and 0.5 km for the mass and the radius, respectively (as chosen in accord with next generation measurements [15]). The variances should also be adjusted according to the real error estimate from observations. Now we obtain the training data set, $(M_i = M_i^{(0)} + \Delta M_i, R_i = R_i^{(0)} + \Delta R_i)$. We call this pair of M_i and R_i an ‘‘observation’’. We repeat this procedure to make 100 observations (denoted by n_s later, and the choice of n_s is arbitrary if large enough for learning) for each EoS, and finally, we have prepared $(1948 \text{ EoSs}) \times (n_s \text{ observations}) = 194800$ training data

Layer index	Nodes	Activation
0	30	N/A
1	60	ReLU
2	40	ReLU
3	40	ReLU
4	5	tanh

TABLE I. Our neural network design in this work. In the zeroth layer 30 nodes correspond to input 15 points of the mass and the radius. In the last layer 5 nodes correspond to 5 output parameters of the EoS.

in this work.

For numerics we make use of a Python library, Keras [22] with TensorFlow [23] as a backend. The design of our neural network is summarized in Tab. I. Our purpose is to construct neural network that can give us one EoS in the output side in response to one observation, (M_i, R_i) ($i = 1, \dots, 15$) in the input side. Thus, in the zeroth layer 30 nodes should match 15 M - R points (30 input data). For the practical reason we sort 30 data points by their masses in ascending order. The output nodes for the prediction target in the last layer correspond to 5 (sound velocity) parameters characterizing an EoS. We find that the learning proceeds faster if data are normalized appropriately; we use M_i/M_{norm} and R_i/R_{norm} with $M_{\text{norm}} = 3M_{\odot}$ and $R_{\text{norm}} = 20$ km.

We choose the activation function at the output layer as $\sigma^{(4)}(x) = \tanh(x)$ since the speed of sound is automatically bounded in $[0, 1]$. For other layers we choose the ReLU, i.e. $\sigma^{(k)}(x) = \max\{0, x\}$ ($k = 1, 2, 3$), which is known to evade the vanishing gradient problem. We specify the loss function as `msle`, that is, the mean square log of prediction errors and choose the fitting method as Adam [24] with the batch size 100. To capture the essence of the problem, the complexity of layers and nodes should be sufficiently large. Simultaneously, to avoid the overfitting problem, and to train neural network within a reasonable time, the number of layers and nodes should not be too large. We found good performance with the node numbers greater than the input node number on the first layer.

The neural network is optimized to fit the training data, but it must have a predictive power for independent data. To test it, we need “validation data” which can be regarded as mock data for the neutron star observation. We generate 200 EoSs, among which 196 EoSs pass the massive neutron star condition. We sample just one observation for each EoS, unlike 100 observations for training data, to mimic real observational situations.

Figure 2 shows typical behavior of the loss function for the training data (dashed lines) and the validation data (solid lines) as a function of training time in units of epoch which represents a single scan of the entire train-

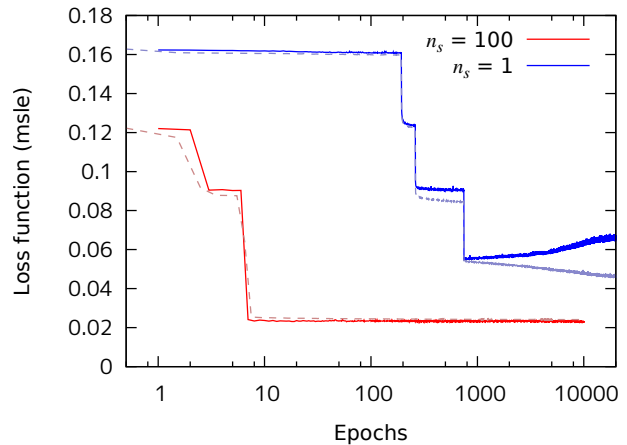


FIG. 2. Loss function estimated for the training data (dashed lines) and the validation data (solid lines) as functions of the epoch. The observation number is denoted by n_s .

ing data. The red solid and dashed lines show the results with $n_s = 100$, i.e. 194800 data set, where n_s is the observation number per EoS. The dashed line is the loss function for the training data minimized through learning, and the solid line is the loss function for the validation data showing the performance of neural network. We monitor the whole history of these quantities over epochs, which is useful to judge when the training is optimally stopped before overfitting. We see that the training is completed within 10 epochs for this example in Fig. 2. For the test purpose to see the efficiency improved by n_s , we also show results with $n_s = 1$ by the blue solid and dashed lines in Fig. 2. The faster learning with $n_s = 100$ than $n_s = 1$ can be explained by data set sizes (194800 for $n_s = 100$ and 1948 for $n_s = 1$). It is important to emphasize that introducing large n_s in our proposal can reduce the computational cost needed to increase the data set size. Interestingly, moreover, the validation loss function for $n_s = 1$ shows overfitting; in general, the loss function for the training data monotonically decreases. For the validation data, however, it may not necessarily decrease and increasing behavior is seen for $n_s = 1$ for epochs $\gtrsim 1000$. This significant separation of training and validation loss functions signals overfitting and then the predicted output could largely deviate from the true answer. We learn from Fig. 2 that the overfitting problem is also cured by $n_s \gg 1$.

Once the loss function converges, we can use the trained neural network to infer an EoS from an observation of 15 M - R points. We picked two examples for Fig. 3. Later, we will quantify the overall performance and for the moment we shall discuss these examples. In Fig. 3 the dashed lines represent randomly generated EoSs. We see that two EoSs are identical in the low density region because SLy is employed at $\rho \leq \rho_0$. We sampled 15 points as shown in Fig. 4, which mimic an

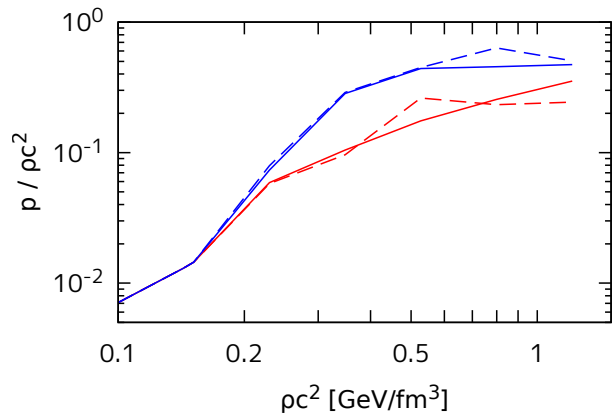


FIG. 3. Two examples of the randomly generated EoSs (dashed lines) and the machine learning outputs (solid lines) reconstructed from one observation of 15 M - R points [see Fig. 4 for actual (M_i, R_i)].

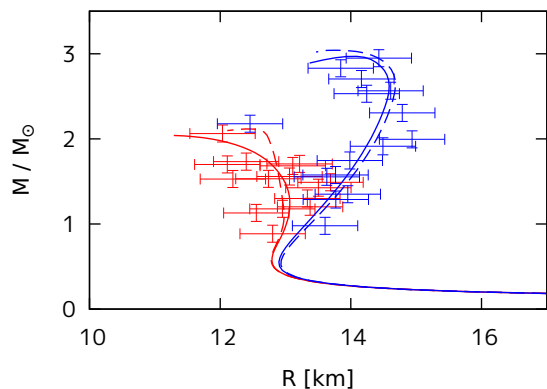


FIG. 4. Randomly sampled 15 data points and the M - R relations with the reconstructed EoS (solid lines) and the original EoS (dashed lines). The red and blue colors correspond to two EoSs shown with the same color in Fig. 3.

observation with error deviations from the genuine M - R relation (which is shown by the dashed lines). Thus, each set of 15 points is considered as mock data of the neutron star observation. Since the neural network learns through the training data that the observation contains errors, the most likely EoS is reconstructed from one observation of 15 points with errors. The reconstructed EoSs are depicted by solid lines in Fig. 3. We can see that the reconstructed EoSs agree quite well with the original EoSs for these examples. It would also be interesting to make a comparison of the M - R relations corresponding to the original and reconstructed EoSs. The solid and dashed lines in Fig. 4 represent the M - R relations calculated with the original and reconstructed EoSs, respectively. Since the EoSs look consistent in Fig. 3, the original and reconstructed M - R relations are close to each other.

Mass (M_\odot)	0.6	0.8	1.0	1.2	1.4	1.6	1.8
RMS (km)	0.16	0.12	0.10	0.099	0.11	0.11	0.12

TABLE II. Root mean square of radius deviations for fixed masses.

For other EoSs in validation data, the corresponding M - R curves are reconstructed well similarly to examples discussed above. To quantify the overall reconstruction accuracy, we calculated the root mean square (RMS) of radius deviations using 196 validation data for several masses as shown in Tab. II. We defined the RMS from the deviations between not the observational data points but the genuine and reconstructed M - R relations (i.e. distances between the solid and the dashed lines in Fig. 4), that is, $\delta R(M) = R^{(\text{rec})}(M) - R^{(0)}(M)$. The RMS values in Tab. II are around ~ 0.1 km for all masses! This indicates that our method works surprisingly good; remember that data points have random fluctuations by $\Delta R \sim 0.5$ km. It should be noticed that, even without neutron stars around $M = 0.6$ – $0.8M_\odot$ in our setup, the RMS of the corresponding radii are still reconstructed within the accuracy of the order ~ 0.1 km.

Finally, let us comment on the relation to Bayesian analysis using symbolic notations. In our analysis we parametrized the EoS by $\theta := \{c_{s,i}^2\}$, which spans parameter space Θ , and generated EoSs by a probability distribution $\Pr(\theta)$. Then, we sampled $\mathcal{D} = \{(M_i, R_i)\}$ by an observational distribution, $\Pr(\mathcal{D}|\theta)$ for each EoS. The neural network is a function f to obtain an EoS from data points, i.e. $f(\mathcal{D}|\mathbf{W}) \in \Theta$, where \mathbf{W} represents the fitting parameters. The training is actually a process to minimize the following loss function:

$$\langle \ell[f] \rangle = \int d\theta d\mathcal{D} \Pr(\theta) \Pr(\mathcal{D}|\theta) \ell(\theta, f(\mathcal{D})). \quad (3)$$

Here, let us translate Bayesian analysis into the above language. In Bayesian analysis a prior distribution of the EoS is assumed to be $\Pr(\theta)$. The posterior EoS distribution is obtained by Bayesian updating; $\Pr(\theta|\mathcal{D}) \propto \Pr(\theta) \Pr(\mathcal{D}|\theta)$. To determine the most likely EoS, we can use the MAP (maximum a posteriori) estimator,

$$f_{\text{MAP}}(\mathcal{D}) = \arg \max_{\theta} [\Pr(\theta) \Pr(\mathcal{D}|\theta)]. \quad (4)$$

This can be interpreted as an approximation of f that minimizes Eq. (3). This means that machine learning encompasses Bayesian analysis as a particular limit. Hence, an advantage of machine learning over Bayesian analysis lies in the direct design of the loss function or optimization target, suited for problems under consideration. We emphasize the generality of our method which can be applied, with a little effort, to any underdetermined problems; an efficient procedure to find the most likely solution optimized with insufficient information and limited

precision.

In this work we parametrized the EoSs with five-segment piecewise polytrope, and assumed a uniform distribution of sound velocity in each segment to generate the training and the validation data. We trained five-layered neural network to obtain successful results. Important future works include systematic investigations of performance and training costs which depend on the EoS parametrization, training and validation data distributions, and the neural network design. The currently formulated method is ideal for forthcoming neutron star observations, but for the moment the available data spread over M - R plane with some probability distribution. We are making progress to adapt our method to deal with such data, which will be reported elsewhere.

K. F. thanks Andrew Steiner for useful discussions. K. F. and K. M. are partially supported by JSPS KAKENHI Grant No. 15H03652 and 15K13479.

-
- [1] G. Aarts, *Proceedings, 13th International Workshop on Hadron Physics: Angra dos Reis, Rio de Janeiro, Brazil, March 22-27, 2015*, *J. Phys. Conf. Ser.* **706**, 022004 (2016), [arXiv:1512.05145 \[hep-lat\]](#).
- [2] G. Baym, T. Hatsuda, T. Kojo, P. D. Powell, Y. Song, and T. Takatsuka, (2017), [arXiv:1707.04966 \[astro-ph.HE\]](#).
- [3] P. Demorest, T. Pennucci, S. Ransom, M. Roberts, and J. Hessels, *Nature* **467**, 1081 (2010), [arXiv:1010.5788 \[astro-ph.HE\]](#); E. Fonseca *et al.*, *Astrophys. J.* **832**, 167 (2016), [arXiv:1603.00545 \[astro-ph.HE\]](#); J. Antoniadis *et al.*, *Science* **340**, 6131 (2013), [arXiv:1304.6875 \[astro-ph.HE\]](#).
- [4] K. Fukushima and T. Hatsuda, *Rept. Prog. Phys.* **74**, 014001 (2011), [arXiv:1005.4814 \[hep-ph\]](#); C. Schmidt and S. Sharma, *J. Phys.* **G44**, 104002 (2017), [arXiv:1701.04707 \[hep-lat\]](#).
- [5] K. Masuda, T. Hatsuda, and T. Takatsuka, *Astrophys. J.* **764**, 12 (2013), [arXiv:1205.3621 \[nucl-th\]](#); D. E. Alvarez-Castillo, S. Benic, D. Blaschke, and R. astowiecki, *Proceedings, 31st Max Born Symposium and HIC for FAIR Workshop : Three Days of critical behaviour in hot and dense QCD: Wroclaw, Poland, June 14-16, 2013*, *Acta Phys. Polon. Supp.* **7**, 203 (2014), [arXiv:1311.5112 \[nucl-th\]](#); K. Fukushima and T. Kojo, *Astrophys. J.* **817**, 180 (2016), [arXiv:1509.00356 \[nucl-th\]](#).
- [6] T. Schäfer and F. Wilczek, *Phys. Rev. Lett.* **82**, 3956 (1999), [arXiv:hep-ph/9811473 \[hep-ph\]](#); M. G. Alford, J. Berges, and K. Rajagopal, *Nucl. Phys.* **B558**, 219 (1999), [arXiv:hep-ph/9903502 \[hep-ph\]](#); K. Fukushima, *Phys. Rev.* **D70**, 094014 (2004), [arXiv:hep-ph/0403091 \[hep-ph\]](#); T. Hatsuda, M. Tachibana, N. Yamamoto, and G. Baym, *Phys. Rev. Lett.* **97**, 122001 (2006), [arXiv:hep-ph/0605018 \[hep-ph\]](#).
- [7] F. Özel and P. Freire, *Ann. Rev. Astron. Astrophys.* **54**, 401 (2016), [arXiv:1603.02698 \[astro-ph.HE\]](#).
- [8] R. C. Tolman, *Phys. Rev.* **55**, 364 (1939); J. R. Oppenheimer and G. M. Volkoff, *Phys. Rev.* **55**, 374 (1939).
- [9] H. Sotani and T. Tatsumi, *Mon. Not. Roy. Astron. Soc.* **447**, 3155 (2015), [arXiv:1412.4610 \[astro-ph.HE\]](#).
- [10] L. Lindblom, *Astrophys. J.* **398**, 569 (1992).
- [11] K. Schertler, C. Greiner, J. Schaffner-Bielich, and M. H. Thoma, *Nucl. Phys.* **A677**, 463 (2000), [arXiv:astro-ph/0001467 \[astro-ph\]](#).
- [12] M. G. Alford and A. Sedrakian, *Phys. Rev. Lett.* **119**, 161104 (2017), [arXiv:1706.01592 \[astro-ph.HE\]](#).
- [13] L. Lindblom, *Phys. Rev.* **D82**, 103011 (2010), [arXiv:1009.0738 \[astro-ph.HE\]](#); L. Lindblom and N. M. Indik, *Phys. Rev.* **D89**, 064003 (2014), [Erratum: *Phys. Rev.* D93, no.12, 129903 (2016)], [arXiv:1310.0803 \[astro-ph.HE\]](#).
- [14] J. S. Read, B. D. Lackey, B. J. Owen, and J. L. Friedman, *Phys. Rev.* **D79**, 124032 (2009), [arXiv:0812.2163 \[astro-ph\]](#).
- [15] F. Özel, G. Baym, and T. Guver, *Phys. Rev.* **D82**, 101301 (2010), [arXiv:1002.3153 \[astro-ph.HE\]](#); Raithel, Carolyn A. and Özel, Feryal and Psaltis, Dimitrios, *Astrophys. J.* **844**, 156 (2017), [arXiv:1704.00737 \[astro-ph.HE\]](#).
- [16] A. W. Steiner, J. M. Lattimer, and E. F. Brown, *Astrophys. J.* **722**, 33 (2010), [arXiv:1005.0811 \[astro-ph.HE\]](#).
- [17] D. Alvarez-Castillo, A. Ayriyan, S. Benic, D. Blaschke, H. Grigorian, and S. Typel, *Eur. Phys. J.* **A52**, 69 (2016), [arXiv:1603.03457 \[nucl-th\]](#).
- [18] L.-G. Pang, K. Zhou, N. Su, H. Petersen, H. Stöcker, and X.-N. Wang, (2016), [arXiv:1612.04262 \[hep-ph\]](#).
- [19] Z. M. Niu and H. Z. Liang, *Phys. Lett.* **B778**, 48 (2018), [arXiv:1801.04411 \[nucl-th\]](#).
- [20] Raithel, Carolyn A. and Özel, Feryal and Psaltis, Dimitrios, *Astrophys. J.* **831**, 44 (2016), [arXiv:1605.03591 \[astro-ph.HE\]](#).
- [21] F. Douchin and P. Haensel, *Astron. Astrophys.* **380**, 151 (2001), [arXiv:astro-ph/0111092 \[astro-ph\]](#).
- [22] F. Chollet, “Keras: Deep learning library for theano and tensorflow,” <https://github.com/fchollet/keras> (2015).
- [23] M. Abadi *et al.*, (2016), [arXiv:1605.08695 \[cs.DC\]](#).
- [24] D. P. Kingma and J. Ba, *CoRR abs/1412.6980* (2014), [arXiv:1412.6980](#).